



# Enhancing anti-tumor therapy with agmatine-cholesterol conjugate liposomes: in vitro and in vivo evidence

Yanzhi Wang<sup>1</sup> · Linchao Wang<sup>1,2</sup> · Hanyue Chang<sup>1</sup> · Qing Shen<sup>1</sup> · Sai Zhang<sup>1</sup> · Shanshan Sun<sup>1</sup> · Ying Liu<sup>3</sup> · Jiaxin Zheng<sup>1</sup> · Hongmin Liu<sup>1</sup>

Accepted: 3 September 2023 / Published online: 27 September 2023  
© Controlled Release Society 2023

## Abstract

In this study, we synthesized a novel compound, agmatine-cholesterol conjugate (AG-Chol), to enhance the anti-tumor activity of drug-loaded liposomes. We replaced cholesterol with AG-Chol in preparing doxorubicin hydrochloride (DOX) liposomes by using an active loading method for DOX. We assessed the physical and chemical properties of the resulting AG-Liposomes and evaluated their efficacy in vitro and in vivo. The results showed that AG-Liposomes were stable with high encapsulation efficiency. Compared with the control liposomes, AG-Liposomes exhibited a slower drug release rate in the release medium at pH 6.8. The in vitro cell experiments demonstrated that AG-Liposomes had higher tumor cell uptake rate, stronger migration inhibition rate, higher apoptosis rate, better anti-clonogenic ability, and higher lysosome escape ability than the control liposomes. In vivo distribution results demonstrate that liposomes prepared with AG-Chol instead of cholesterol can significantly enhance their tumor targeting abilities and reduce their distribution to non-targeted sites. In vivo tumor suppression experiments showed that AG-Liposomes had a higher tumor suppression rate than the control liposomes without causing apparent toxicity to normal tissues, as evidenced by histological staining. Therefore, substituting cholesterol with AG-Chol in the preparation of liposomes can result in enhanced lysosome escape, improved tumor targeting, and increased efficacy of anti-tumor drugs.

**Keywords** Doxorubicin hydrochloride · Agmatine-cholesterol conjugate · Liposomes · Lysosomal escape · Tumor target · MGC 803

## Introduction

The development of new excipients is essential for the innovation of nano-formulations. For instance, the emergence of various PEGylated drugs or carriers, materials with a

targeted modification, and new types of carriers has facilitated the powerful exploration of nano-formulations' potential [1–4]. However, many studies encounter issues such as poor reproducibility large-scale production, excessive components, or high toxicity of carrier materials. Therefore, few nano-formulations have progressed clinical trials and been approved [5]. We should dedicate more energy to excipients and preparations with more excellent clinical development prospects.

Liposomal formulations are one of the earliest nano-formulations on the market. Drugs such as doxorubicin and paclitaxel have been successfully encapsulated in liposomes and have been used in the clinic [5]. The safety of liposome preparations has been confirmed, and their drug-carrying capacity, preparation methods and other technologies are mature. As a result, the utilization of new excipients for liposomal preparations may facilitate clinical translation. A highly successful case is the development of mRNA COVID-19 vaccines by Pfizer-BioNTech or Moderna Therapeutics [6, 7]. They are based on the

✉ Yanzhi Wang  
wangyz@zzu.edu.cn

✉ Jiaxin Zheng  
zjx1224@163.com

✉ Hongmin Liu  
liuhm@zzu.edu.cn

<sup>1</sup> State Key Laboratory of Esophageal Cancer Prevention & Treatment, Key Laboratory of Advanced Drug Preparation Technologies, Henan Key Laboratory of Drug Quality Control & Evaluation, School of Pharmaceutical Sciences, Ministry of Education of China, Zhengzhou University, Zhengzhou, China

<sup>2</sup> Jining No. 1 People's Hospital, Jining, China

<sup>3</sup> Hainan General Hospital, Hainan Affiliated Hospital of Hainan Medical University, Haikou, China

formulation of liposomes with the addition of ionizable lipids, which ultimately form lipid-encapsulated lipid nanoparticles carrying mRNA [8, 9].

Liposomes are mainly composed of phospholipids and cholesterol. Both natural and synthetic phospholipids have been used in liposome preparations [10, 11]. PEGylated phospholipids have been applied in the clinic, and liposomes prepared with this adjuvant have a longer circulation time in the blood and circulatory system, which enables the accumulation of the pharmaceutical preparation at the diseased site through passive targeting and other mechanisms [12, 13]. Furthermore, there has been a focus on modifying cholesterol [14]. For example, compounds containing cholesterol groups and biguanides have been synthesized and added to liposome or nanoparticle preparations [15, 16]. These compounds may assist in the quick internalization of liposomes or nanoparticles into tumor cells and promote their escape from lysosomes. However, these compounds also exhibit some antitumor effects and toxicity that may impede their clinical use.

From the perspective of facilitating research and clinical development, we aim to develop a guanidine-cholesterol conjugate with high biological safety. The ideal compound should not exhibit anti-cancer activity but possess the beneficial properties associated with guanidine groups. This conjugate could potentially replace cholesterol in the formation of stable drug-loading liposomes with phospholipids. Our interest has been aroused by Agmatine, one of the degradation products of Metformin in the intestine [17]. In this study Agmatine was found to have the potential to extend the lifespan of nematodes and fruit flies, and may contribute to extending human lifespan [17]. Therefore, our objective is to synthesize a cholesterol-agmatine conjugate, designated as AG-Chol. Some degradation products of AG-Chol, namely cholesterol and Agmatine, do not increase the toxicity of AG-Chol. This property supports the safety profile of AG-Chol. Nonetheless, the toxicity of the conjugate may not always correspond with that of its degradation products. To explore the role of AG-Chol and test our hypothesis, we synthesized AG-Chol and used it to prepare doxorubicin liposomes by replacing cholesterol. We selected gastric cancer MGC 803 cells as the model cell line and performed a series of *in vitro* and *in vivo* investigations, including assessments of cytotoxicity, lysosomal escape, apoptosis, western blot assays, and tumor inhibition.

## Materials and methods

### Materials

Doxorubicin hydrochloride (DOX), cholesteryl chloroformate, monocyandiamide, ammonium sulphate and

1,4-butanediamine were obtained from Shanghai Aladdin Bio-Chem Technology Co., Ltd. (Shanghai, China). Egg yolk lecithin (PC-98 T) was bought from A.V.T.(Shanghai) Pharmaceutical Technology Co., Ltd. (Shanghai, China). MTT were provided by Dalian Meilun Biotechnology Co., Ltd. (Dalian, China). LysoSensor™ Green DND-189 was obtained from Shanghai Yisheng biology Co., Ltd. (Shanghai, China). IR-780 iodide was purchased from Sigma-Aldrich (Shanghai, China). 4',6-diamidino-2-phenylindole (DAPI), DNA Content Quantitation Assay (cell cycle), Hoechst 33342, Pierce ECL Western Blotting Substrate, Diaminobenzidine (DAB), eosin and hematoxylin were bought from Solarbio Science & Technology Co., Ltd. (Beijing, China). Annexin V-FITC/PI Apoptosis Detection Kit, Bax, Bcl-2, cleaved caspase-9, cleaved caspase-3 and GAPDH were acquired from Shenyang Wanlei Biotechnology Co., Ltd. (Shenyang, China). Other chemicals were obtained from Tianjin Sairuifu chemical plant (Tianjin, China).

### Cell culture

MGC 803 cells (iCell Bioscience Inc) and H22 cells (Wuhan Procell Life Science&Technology Co.,Ltd.) were cultured in RPMI-1640 culture medium containing 0.1 mg/ml streptomycin, 100 U/ml penicillin and 10% fetal bovine serum (FBS) in a humidified incubator (95% relative humidity, 5% CO<sub>2</sub>, 37 °C).

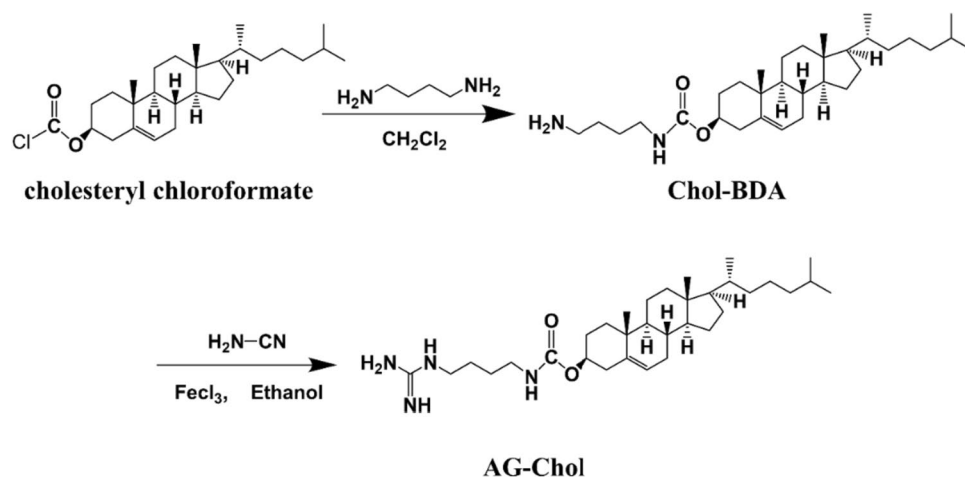
### Establishment of cancer model mice

Swiss mice (18–22 g, male) were bought from Henan experimental animal center. H22 cells ( $1 \times 10^6$ ) dispersed in 0.1 ml saline were subcutaneously injected into the armpit of the mice. The experiment was performed when tumors reached  $\sim 100 \text{ mm}^3$  one week later. All animal studies were carried out following protocols approved by Institutional Animal Care and under the supervision of the Animal Ethics Committee of Zhengzhou University.

### Synthesis of AG-Chol

The synthesis of AG-Chol (Mw = 542.85) was made using the method outlined in Fig. 1. The process consisted of two stages. During the first stage, 0.45 g cholesteryl chloroformate (Mw = 449.12) was dissolved in 4 mL of anhydrous dichloromethane and 0.3 mL of pyridine. The above solution was added dropwise to a stirring cold solution (4 °C) of 8 ml 1,4-butanediamine (Mw = 88.15) in 8 ml dichloromethane. The mixture underwent stirring for a duration of 24 h at 4 °C, followed by filtration. The solvent was subsequently eliminated, and the remaining substance was precipitated three times by adding acetonitrile and centrifuging the mixture.

**Fig. 1** Synthetic route of AG-Chol



The final precipitation was washed with ultrapure water and dried to obtain the cholesterol butane diamine conjugate (Chol-BDA) ( $M_w = 500.81$ ) [16]. In the second stage, 236.2 mg Chol-BDA, 61.36 mg anhydrous ferric chloride ( $M_w = 162.2$ ), and 178.41 mg monocyanamide ( $M_w = 42.04$ ) (molar ratio = 1: 0.8: 9) were dissolved in 5 ml ethanol and stirred for 12 h at 120 °C under nitrogen protection. After the reaction, the liquid was centrifuged to remove ferric chloride, and AG-Chol was obtained by silica gel column chromatography (Dichloromethane: methanol = 20:1). The purity of AG-Chol was verified by conducting  $^1\text{H}$  and  $^{13}\text{C}$  NMR analyses using  $\text{DMSO-d}_6$  and  $\text{CDCl}_3$  at 400 MHz and 100 MHz, respectively.

### Preparation of DOX liposomes

We prepared DOX-loaded liposomes by combining the thin-film dispersion ultrasonic method with the ammonium sulfate gradient method [18]. To do this, we dissolved 15 mg of egg yolk lecithin (PC-98 T) and 5 mg AG-Chol/Cholesterol in a mixed solution of 2 ml of ethanol and chloroform (1:1, v/v), then evaporated the organic solvent under reduced pressure at 50 °C. The resulting film was mixed with 1 ml of 250 mmol/L ammonium sulfate aqueous solution and ultrasonicated for 5 min (3 s on, 5 s off, 360 W) at 40 °C using an ultrasonic cell crusher (SCIENTZ-IIID, NINGBO SCIENTZ). The liposomes were then dialyzed for 4 h (with water changes every hour) to remove the ammonium sulfate. Finally, 0.2 ml of DOX solution (20 mg/ml) was added to the liposomes and stirred for 1 h at 40 °C to obtain the final DOX liposomes. DOX liposomes containing cholesterol or AG-Chol are named Liposomes and AG-Liposomes, respectively.

### Characterization of DOX liposomes

#### Particle size and zeta potential

The mean diameter, polydispersity index (PDI) and zeta potentials of the liposomes diluted by 4 times volume of water were measured by dynamic light scattering (DLS) analysis using Zetasizer Nano ZS (Malvern Instruments).

#### Surface morphology

The surface morphology of AG-Liposomes was examined by transmission electron microscopy (TEM) with JEOL 100CX II. Briefly, the formulated liquid was diluted tenfold with ultrapure water, and then dropped onto a carbon-coated copper grid placed on filter paper. After 10 min later, 10  $\mu\text{l}$  of 3% uranyl acetate stain was added. Following a 1.5-min staining period, excess staining solution on the copper grid was removed using filter paper. The specimen was then allowed to stand at room temperature for 10 min before being imaged under a TEM.

#### Entrapment efficiency, drug loading and drug release in vitro

**Concentration determination method of DOX** A fluorescence spectrophotometer (RF-5301PC, Japan) was used to determine DOX concentration using an excitation wavelength of 481 nm and an emission wavelength of 579 nm. A standard curve was constructed with fluorescence intensity ( $y$ ) and DOX concentration ( $x$ ) with a relationship of  $y = 27.936x - 1.0654$  (0.05–1  $\mu\text{g/ml}$ ) and an  $R^2$  value of 0.9993. A fresh standard curve was prepared for each experiment ( $n = 3$ ).

**Entrapment efficiency of DOX** The method for determining DOX's total and free drug content in liposomes involves

diluting 200  $\mu\text{l}$  of liposomes with 3.8 ml of methanol, mixing for 1 min with vortex, and sonicating for 20 min. Then, 200  $\mu\text{l}$  of the resulting solution is diluted with methanol to a final volume of 10 ml, and its fluorescence intensity is measured to calculate the total drug content ( $W_{\text{total}}$ ). Another 200  $\mu\text{l}$  of liposomes is centrifuged at 10,000 r/min with a molecular weight cutoff of 3 kDa for 30 min to separate the free drug, and the bottom solution is collected, mixed with methanol to 10 ml, and its fluorescence intensity is measured to calculate the free drug content ( $W_{\text{free}}$ ). The encapsulation efficiency of DOX in the liposomes is then calculated using  $W_{\text{total}}$  and  $W_{\text{free}}$ :

$$\text{Entrapment efficiency (\%)} = \frac{W_{\text{total}} - W_{\text{free}}}{W_{\text{total}}} \times 100\%$$

**DOX loading capacity of AG-Liposomes** Blank liposomes (15 mg EPC, 5 mg AG-Chol, in 1 ml) were prepared to encapsulate different quantities of DOX. The entrapment efficiency was calculated to assess the liposome's loading capacity.

**In vitro release of DOX liposomes** The release of DOX from Liposomes and AG-Liposomes was studied at three pH levels (7.4, 6.8, and 4.5) by incubating the samples at 37 °C with gentle shaking. The solutions were centrifuged at specific intervals (0.5, 2, 4, 6, 8, 10, and 24 h), and the concentration of DOX in the supernatant was measured using the method established in Section “[Concentration determination method of DOX](#)”.

## Comparative study on tissue distribution and targeting of different liposomes

### Preparation of liposomes containing IR780

15 mg of EPC, 1 mg of IR780, and 5 mg of AG-Chol/Cholesterol were dissolved in a mixture of ethanol and chloroform (2 ml, 1:1 v/v) and the organic solvent was evaporated under reduced pressure at 50 °C. The resulting film was then hydrated with 1 ml of PBS and subjected to sonication using an ultrasonic cell crusher (5 m, 3 s on, 5 s off, 360 W) at 40 °C, which produced liposomes containing IR780. IR780 liposomes containing cholesterol or AG-Chol are named 780-Liposomes and 780-AG-Liposomes, respectively.

### Tissue distribution of different liposomes

Swiss mice (18–22 g, male) were subcutaneously inoculated with 1 million H22 cells per 100  $\mu\text{l}$  per mouse in the axilla. Once the tumor volume reached over 100  $\text{mm}^3$ , 780-Liposomes and 780-AG-Liposomes were administered

intravenously at a dose of 5 mg/kg. At 24 h and 48 h post-administration, the animals were anesthetized using intraperitoneal chloral hydrate injection. Subsequently, they were euthanized, and the fluorescence intensity of the heart, liver, lung, spleen, kidney, and tumor was measured using a NIR-II small animal imaging system (FX PRO, Bruker). The imaging parameters included an excitation wavelength of 770 nm, emission wavelength of 830 nm, and exposure time of 20 s. This experiment aimed to investigate the in vivo distribution of various liposomal formulations.

## Tumor cell uptake assay

MGC 803 cells were seeded in 6-well plates at a density of approximately  $1 \times 10^5$  per well and grown for 24 h. Subsequently, the culture medium was substituted with medium that contained 2  $\mu\text{g}/\text{ml}$  of DOX solution, Liposomes, or AG-Liposomes. After being cultured for 1, 2, or 4 h, the cells were fixed with 4% paraformaldehyde and for 15 min, washed with cold PBS solution, and stained with 1 ml of DAPI at room temperature for 10 min. The cells were then mounted on glass slides and their fluorescence was captured using a laser confocal microscope (LSM510, ZEISS).

## Cytotoxicity test of AG-Chol

Three types of cells, including cardiomyocytes H9C2, gastric cancer cells MGC 803, and lung cancer cells A549, were selected to evaluate the cytotoxicity of AG-Chol using the MTT assay. The seeding density of H9C2, MGC 803, and A549 in the 96-well plate were  $4 \times 10^3$  cells/well,  $1 \times 10^3$  cells/well, and  $5 \times 10^3$  cells/well, respectively. After 24 h of incubation, AG-Chol was added to each well at final concentrations ranging from 256  $\mu\text{g}/\text{ml}$  to 4  $\mu\text{g}/\text{ml}$ , followed by another 24 h of incubation. After that, MTT solution was added and the cells were grown in the dark for 4 h. The culture medium was removed and 200  $\mu\text{L}$  of DMSO was added. The mixture was agitated for a duration of 10 min, and the absorbance was subsequently determined at 490 nm using a Synergy HI microplate reader (Biotek). Absorbance was used to calculate cell viability.

## In vitro cell viability of DOX preparations on MGC 803 cells

A MTT assay was conducted to evaluate the in vitro cell viability of MGC 803 cells in response to PBS, DOX solution, Liposomes and AG-Liposomes. MGC 803 cells were seeded in 96-well plates at a density of  $1 \times 10^3$  cells per well and cultured for 24 h. They were then treated with DOX solution or DOX liposomes, and incubated for another 24 or 48 h. The subsequent steps followed the protocol described in Section “[Cytotoxicity test of AG-Chol](#)”. The cell inhibition

rate was determined based on the absorbance values. The CompuSyn software was used to estimate the half maximal inhibitory concentration (IC50).

### In vitro scratch assay

MGC 803 cells were seeded in 6-well plates at a density of  $2 \times 10^5$  cells per well and grown. The culture medium was abandoned when the cells reached near full confluence. Vertical scratches were made using a 200  $\mu$ l pipette tip and the wells were gently washed with PBS. Then, 2 ml of RPMI 1640 medium and the tested preparation were added to each well. Photos of the cells were taken after 0 h and 36 h of incubation. PBS, DOX solution, Liposomes and AG-Liposomes were investigated and compared, with a DOX concentration of 1  $\mu$ g/ml.

### Clonogenic assay

MGC 803 cells were seeded into 6-well plates with a density of  $1 \times 10^3$  cells per well. Following 48 h of incubation, the culture medium was substituted with fresh medium containing one of the test preparations (PBS, DOX solution, Liposomes, and AG-Liposomes). When clones formed in the control group, 1 ml of 4% paraformaldehyde was added to each well and allowed to incubate for 15 min. After being rinsed with PBS solution, each well was stained with 2 ml of 0.1% crystal violet solution for 10 min. Cell pictures were taken after washing with PBS. The study investigated and compared three different concentrations of DOX preparations.

### Tumor cell apoptotic assay

MGC 803 cells were seeded at a density of  $1.7 \times 10^5$  cells per well in a 6-well plate. After 24 h, the cells were washed with PBS and cultured in a medium containing one of the test preparations: PBS, DOX solution, Liposomes and AG-Liposomes. After 24 h of culture, the cells were collected by centrifugation, washed with cold PBS, and mixed with 500  $\mu$ l of  $1 \times$  binding buffer. The cells were then stained with 5  $\mu$ l Annexin-V-FITC dye for 15 min and 5  $\mu$ l PI dye solution for 5 min. The cells that had been stained were examined using a flow cytometer (Epics XL, Beckman Coulter).

### Endosomal escape evaluation

To assess the endo-lysosomal escape ability of the DOX preparations, we tested DOX solution, Liposomes and AG-Liposomes. Briefly,  $1 \times 10^5$  MGC 803 cells were cultured

in 6-well plates and permitted to proliferate for a duration of 12 h before the culture medium was replaced with one containing the DOX preparation. After 4 h, the cells were rinsed three times with cold PBS and stained with LysoSensor™ Green DND-189 (green) and Hoechst33342 (blue) for 20 min each. Fluorescence images were obtained using a laser confocal microscope (LSM510, ZEISS). To further investigate the co-localization of DOX and lysosomes, we used ImageJ software to process the images and obtain data on the grayscale values of the red and green fluorescence signals as a function of position.

### Western blot experiment and analysis

The expression of Bax, Bcl-2, cleaved caspase-9, and cleaved caspase-3 in MGC 803 cells was evaluated using western blot analysis, with GAPDH as the reference protein. The procedure was as follows: MGC 803 cells were cultured in a 10 cm diameter cell culture dish until they covered 70–80% of the dish. The cells were then treated with PBS, DOX solution, Liposomes, or AG-Liposomes (at a DOX concentration of 2  $\mu$ g/ml) for 24 h. After harvesting the cells, their proteins were extracted, separated by 10% SDS-PAGE electrophoresis, and transferred to PVDF membranes. The membranes were cultivated overnight at 4 °C with primary antibodies after being blocked with 5% dry milk, followed by incubation with HRP-labeled secondary antibodies. Chemiluminescent detection was carried out using Pierce ECL Western Blotting Substrate. Each group was run in triplicate, and the optical density of each protein band was analyzed using ImageJ software.

### Tumor growth inhibition study

In this study, Swiss mice bearing subcutaneous H22 tumors were intravenously administered with different formulations every four days, including PBS, DOX solution, Liposomes, or AG-Liposomes at a dose of 5 mg/kg of DOX. The mice were weighed and tumor size was measured using vernier calipers, and a total of three injections were given. Two days after the final injection, the mice were euthanized, and the heart, liver, spleen, kidney, and lung were dissected and weighed. The tumor growth inhibition rate was calculated as  $(1-T/C) \times 100\%$ , where T and C are the mean tumor volumes or weight of the treatment and control groups, respectively. A volume–time curve was plotted to evaluate the therapeutic efficacy of each formulation. The heart, liver, spleen, kidney, and lung were collected for further analysis. The equation to calculate tumor volume is as follows:  $V(\text{mm}^3) = 1/2 \times ab^2$ . Here, ‘a’ represents the length and diameter of the tumor (mm), while ‘b’ denotes the tumor’s shorter diameter (mm).



## H&E staining assay

To assess the toxicity, tissues obtained from the experiment in Section “[Tumor growth inhibition study](#)” were fixed in 4% paraformaldehyde for 48 h and then prepared for H&E staining. The tissue was dehydrated, embedded in paraffin, and sectioned. The sections were stained with eosin and hematoxylin, and then sealed with neutral resin. Finally, they were photographed by an automatic digital slide scanner (PANNORAMIC MIDI II).

## Statistical analysis

Data in this study were given as mean  $\pm$  standard deviation (SD). The difference between the two groups was tested by GraphPad Prism 9 software using One-way ANOVA.  $P < 0.05$  was regarded statistically significant.

## Results and discussion

### Synthesis of AG-Chol

For the purpose of result analysis, AG-Chol was numbered (Fig. 2A) and the product appeared as a white powder (Fig. 2B). The structure of the product was confirmed through proton nuclear magnetic resonance ( $^1\text{H-NMR}$ ) and carbon-13 nuclear magnetic resonance ( $^{13}\text{C-NMR}$ ) spectroscopy, as shown in Fig. 2C, D, respectively. The  $^1\text{H-NMR}$  spectrum displayed all the characteristic proton peaks of AG-Chol, including 7.03 (=N<sub>39</sub>H), 6.55 (N<sub>31</sub>H), 5.86 (C<sub>10</sub>H), 5.32 (N<sub>38</sub>H), and 4.3 (C<sub>4</sub>H). The proton peaks at 7.03, 5.32, and 5.35 in the  $^1\text{H-NMR}$  spectrum were attributed to the guanidinium group. Similarly, the  $^{13}\text{C-NMR}$  spectrum of the product showed characteristic peak shift values of 155.68 (C<sub>37</sub>, C<sub>1</sub>), 138.77 (C<sub>6</sub>), and 121.54 (C<sub>10</sub>), which were consistent with those of AG-Chol. All other peaks in the spectra

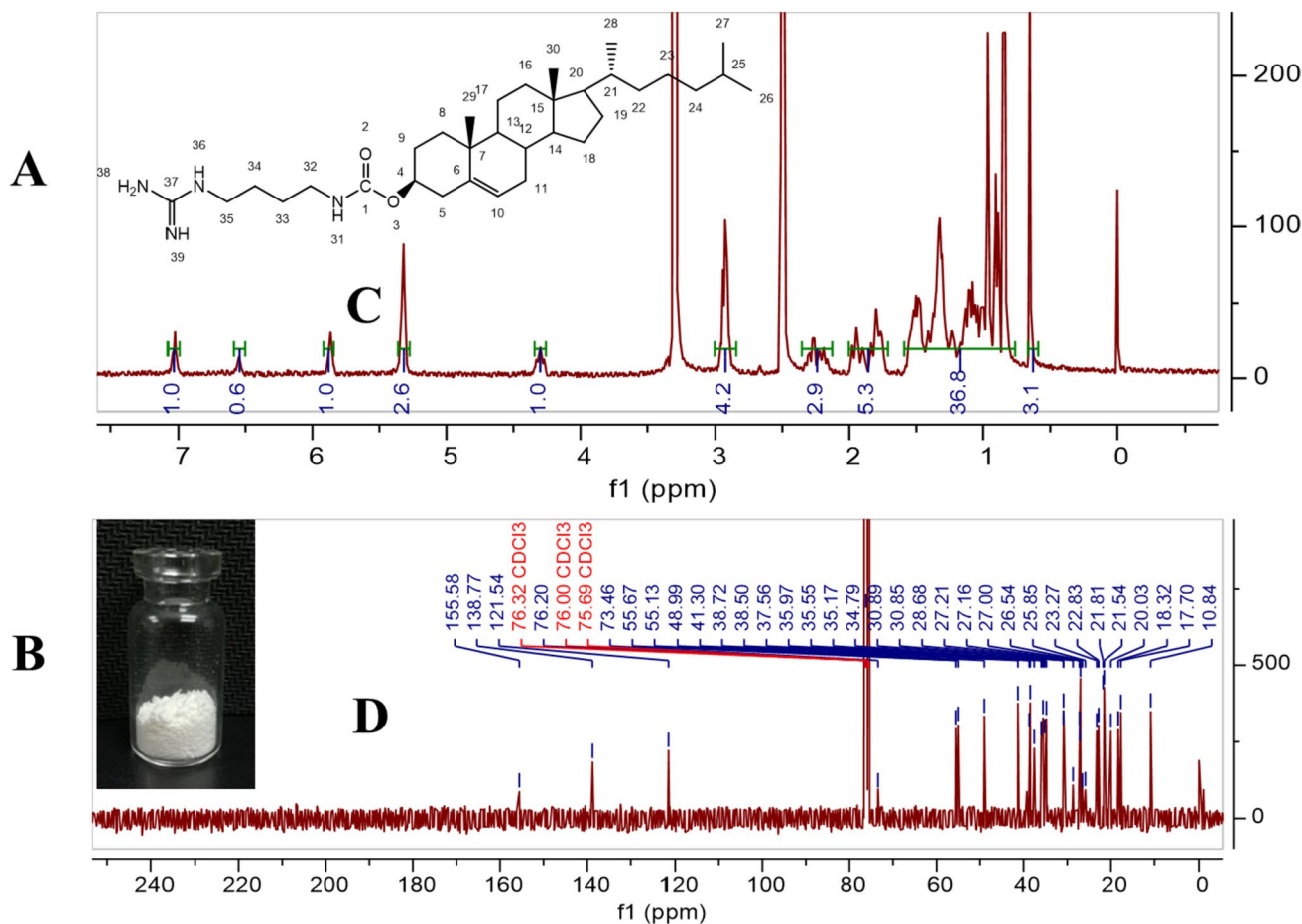


**Fig. 2.**  $^1\text{H-NMR}$  and  $^{13}\text{C-NMR}$  spectra of AG-Chol: **A** Numbered structural formula; **B** Appearance of AG-Chol; **C**  $^1\text{H-NMR}$  spectra and **D**  $^{13}\text{C-NMR}$  spectra of AG-Chol

were also consistent with the structure of AG-Chol, providing further confirmation that the synthesized product is indeed AG-Chol.

### Characterization of DOX liposomes

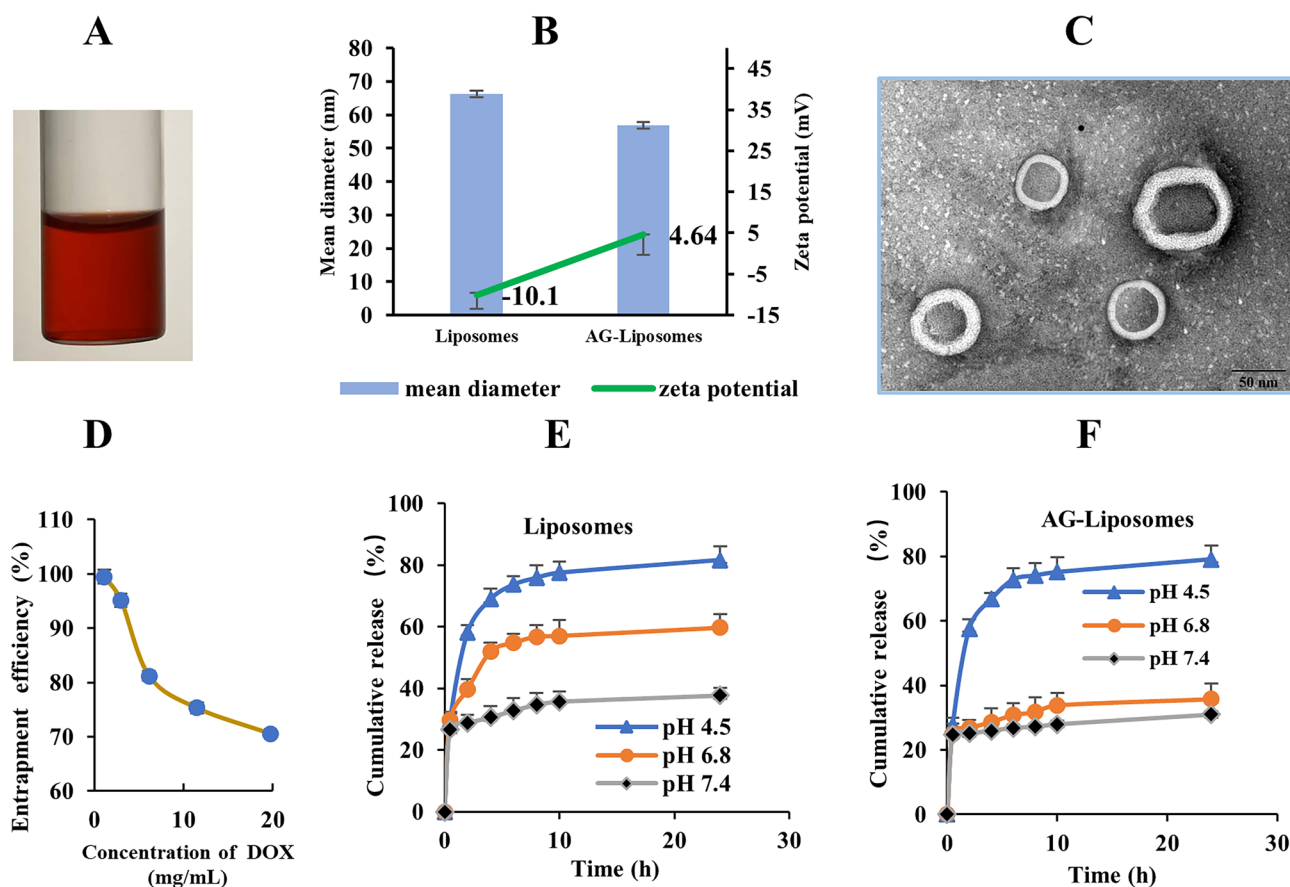
AG-Liposomes are red translucent liquid, as shown in Fig. 3A. Figure 3B compares the mean particle size and zeta potential of AG-Liposomes to the Liposomes produced with cholesterol. The average number diameter of AG-Liposomes was  $56.75 \pm 1.16$  nm, smaller than that of Liposomes ( $66.18 \pm 1.60$  nm), and its mean zeta potential was  $+4.63 \pm 0.08$  mV, compared to  $-10.0 \pm 0.51$  mV for the Liposomes. This may result from AG-Chol's higher hydrophilicity and positive charge than cholesterol, which leads to tighter packing of the phospholipids in the liposomes and positive charge on the liposomes surface.

Figure 3C shows the electron microscopy image of AG-Liposomes that display typical liposome features, consisting of an outer lipid layer and an inner aqueous phase. The thickness of the phospholipid layer appears to be between

5–15 nm, compared to 4–5 nm observed in simple lipid bilayers. This thickening was reported in previous studies of cationic liposomes [11, 19, 20]. The particle size observed through electron microscopy agrees with the size measured using DLS.

Figure 3D shows the entrapment efficiency of DOX in AG-Liposomes with a lipid content of 15 mg/ml. With increasing DOX concentration, the encapsulation efficiency decreases. At DOX concentrations below 4 mg/ml, 6.5 mg/ml, and 20 mg/ml, the entrapment efficiencies are over 90%, 80%, and 70%, respectively. The encapsulation efficiency of DOX in AG-Liposomes meets the required standard compared to the typical marketed formulation of DOX with a concentration of 2 mg/ml. This result indicates that AG-Liposomes can actively load DOX.

After intravenous administration, a fraction of DOX-loaded liposomes circulating in blood penetrate the tumor tissue to interact with the tumor cells via the interstitial fluid of the tumor tissue. The pH values of these environments are approximately 7.4 (blood), 6.8 (tumor interstitial fluid), and 4.5 (tumor cells) [21]. We measured the release of the two



**Fig. 3** Physicochemical characterization of DOX liposomes: **A** The appearance of AG-Liposomes; **B** Mean diameter and zeta potential of control liposomes and AG-Liposomes; **C** TEM images of

AG-Liposomes (bar=50 nm); **D** Entrapment efficiency of AG-Liposomes; **E** Cumulative release of control liposomes and **F** Cumulative release of AG-Liposomes. The error bars presented SD (n=3)

DOX-loaded liposomes at these three pH levels. As shown in Fig. 3E and F, both liposomes show slower release at neutral pH, maintaining high drug loading until reaching the tumor site. Both liposomes exhibit higher cumulative release at acidic pH, facilitating drug delivery to the tumor cells. However, AG-Liposomes have a significantly lower release rate than regular liposomes at pH 6.8, improving their stability in the tumor interstitium prior to interacting with the tumor cells.

### Cytotoxicity of AG-Chol

We selected two tumor cell lines, MGC 803 and A549, and one cardiac cell line, H9C2, to assess the toxicity of AG-Chol on these cells using the MTT assay. Figure 4A shows that AG-Chol was least toxic to A549 cells, with no effect on viability at 256  $\mu\text{g/ml}$ .

AG-Chol was also mildly toxic to MGC 803 cells, with viability above 85% at concentrations below 256  $\mu\text{g/ml}$ , indicating relative safety in this range. However, cardiac cells showed decreased viability (<70%) at AG-Chol concentrations above 128  $\mu\text{g/ml}$ , implying cardiotoxicity. This may reflect the higher susceptibility of cardiac cells to AG-Chol toxicity. AG-Chol had no significant effect on cardiac cell proliferation at concentrations around 64  $\mu\text{g/ml}$  or lower.

Overall, we synthesized a compound with negligible or low cytotoxicity to tumor and normal cells. Given its application at a 3:2 ratio with DOX in the optimal formulation, AG-Chol is not cytotoxic to normal cells and tumor cells at the usual DOX dose. Moreover, DOX liposomes distribute slower to tissues than DOX solution, and their  $C_{\text{max}}$  in the heart is about 50–60% of that of solution, thus liposomes can significantly reduce the cardiac toxicity of agents [22]. Therefore, this compound may be a non-cytotoxic excipient for DOX liposome preparation. Our results also support

our hypothesis of lower cytotoxicity of AG-Chol than MET-Chol. At usual doses, AG-Chol does not affect the viability of normal and tumor cells, facilitating further development.

### In vitro cell viability of DOX preparations on MGC 803 cells

We evaluated the toxicity of three DOX formulations (DOX solution, Liposomes and AG-Liposomes) on MGC 803 cells (Fig. 4B and C). Overall, both liposome formulations were more toxic than the DOX solution, especially at high concentrations at 24 h (Fig. 4B). After 48 h, liposomes were significantly more toxic than the DOX solution at all concentrations (Fig. 4C). The IC<sub>50</sub> values for MGC 803 cells treated with DOX solution, Liposomes and AG-Liposomes were  $2.57 \pm 0.04$   $\mu\text{g/ml}$ ,  $1.35 \pm 0.02$   $\mu\text{g/ml}$  and  $0.56 \pm 0.01$   $\mu\text{g/ml}$  at 24 h; and  $0.43 \pm 0.01$   $\mu\text{g/ml}$ ,  $0.08 \pm 0.0003$   $\mu\text{g/ml}$  and  $0.04 \pm 0.001$   $\mu\text{g/ml}$  at 48 h, respectively. AG-Liposomes had about half the IC<sub>50</sub> value of Liposomes indicating increased cellular toxicity of AG-Chol modified liposomes to tumor cells.

### Tumor targeting and tissue distribution of different liposomes

We utilized imaging technology to compare the in vivo distribution of two IR780-loaded liposomes following intravenous administration at 24 and 48 h (Fig. 5A and B). IR780 fluorescence was higher in tumors than in several normal tissues at both time points. Furthermore, AG-Liposomes had significantly higher fluorescence in tumors than Liposomes at both time points. Additionally, it is noteworthy that AG-Liposomes had lower fluorescence in normal tissues like the heart, liver, spleen, lung, and kidney than that of Liposomes. This difference

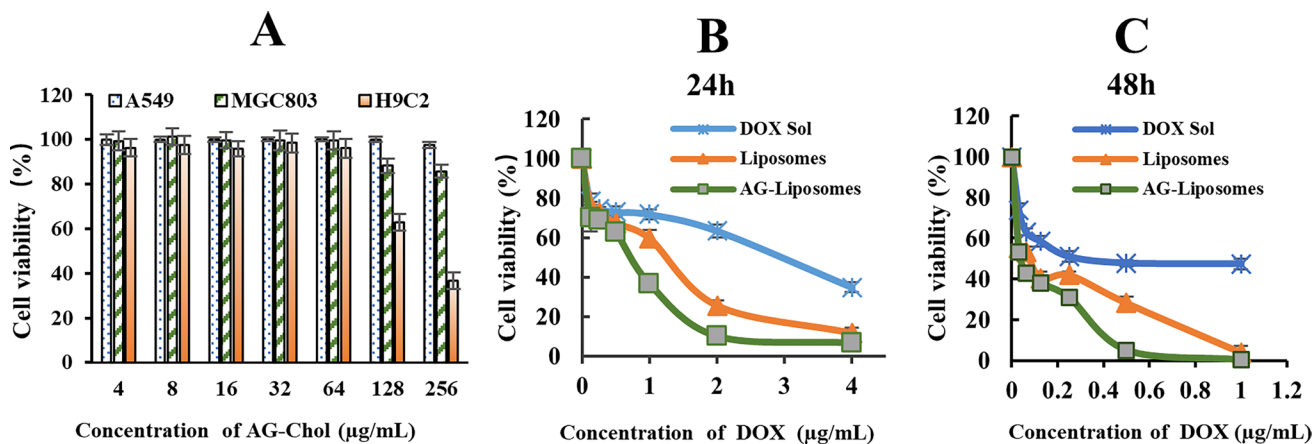


**Fig. 4** Cytotoxicity test results: **A** Cell viability of A 549, MGC 803 and H9C2 treated by different concentrations of AG-Chol; **B** Cell viability of MGC 803 treated with DOX preparations for 24 h and **C** Cell viability of MGC 803 treated with DOX preparations for 48 h



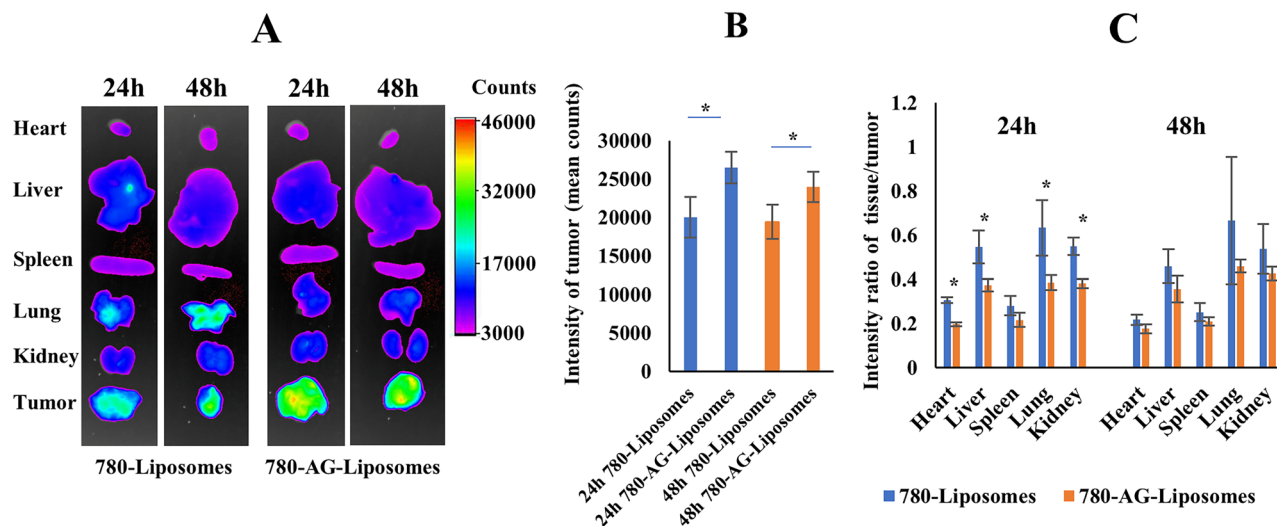


**Fig. 5** NIR images of organs after iv administration of different DOX liposomes: **A** EX vivo NIR images of organs; **B** Statistical analysis of the tumor intensities treated with different liposomes for 24 h

and 48 h and **C** Statistical analysis of intensity ratio of tissue/tumor treated with different liposomes at 24 h and 48 h (n=3). \*  $p < 0.05$

was more pronounced at 24 h (Fig. 5C). These results showed that AG-Chol liposomes can improve tumor targeting and decrease distribution to non-targeted sites. This targeted distribution characteristic will improve the therapeutic effect of anti-tumor preparations while reducing side effects. AG-Liposomes target the heart less than liposomes, which reduces worries about the harmful effects of AG-Chol and DOX on the heart.

Compared to conventional nanocarriers, many targeted or long-circulating modified nanocarriers accumulate more in tumors and other tissues like the liver, lungs and spleen. For instance, nanocarriers modified with folic acid [23–26], N-(2-aminoethyl)-4-methoxybenzamide [27], anisamide [27, 28], or hyaluronic acid have this feature [29, 30]. Thus, some preparations have high tumor fluorescence not only because of better targeting, but also because of more accumulation from longer body retention or slower degradation. Their relative tumor uptake may not be much higher. In contrast, our AG-Chol modified liposomes demonstrate excellent tumor targeting effects, suggesting that AG-Chol is a potential substance for more research and development.

### Cell scratch, cloning and apoptosis experiments

We used a scratch test to assess how different DOX preparations affect cell migration (Fig. 6A, B). All three DOX preparations lowered cell migration significantly. AG Liposomes, Liposomes, and the solution had migration rates of  $33.5 \pm 0.71\%$ ,  $10.0 \pm 0.96\%$ , and  $1.2 \pm 0.80\%$ , respectively.

The clonogenic assay results show that higher DOX concentration in each preparation led to more clonogenic

inhibition (Fig. 6C). AG-Liposomes had the highest efficacy, followed by Liposomes, and then the solution.

The apoptosis experiment results showed that at  $0.5 \mu\text{g}/\text{mL}$  concentration, AG-Liposomes, Liposomes, and the solution had apoptosis rates of  $32.12 \pm 2.62\%$ ,  $22.97 \pm 1.58\%$ , and  $9.97 \pm 1.25\%$ , respectively (Fig. 6D, E).

These cell experiments suggest that AG-Liposomes reduced cell migration and cloning more effectively than Liposomes and the solution did, and induced more cell apoptosis.

### Cell uptake and lysosomal escape

To determine the effect of AG-Chol on the uptake and lysosomal escape of liposomes by tumor cells, we performed cell experiments using DOX as a model drug, as shown in Fig. 7. As illustrated in the figure, tumor cells took up more liposomes than DOX solution. These findings indicate that the liposome formulation significantly enhanced the uptake rate of tumor cells and that AG-Chol addition further increased the uptake of DOX liposomes. This is likely due to the positive charge imparted on the liposome surface by AG, which facilitates interaction with the negatively charged cell surface and subsequent entry into the cell via endocytosis and other pathways [31].

Regarding the lysosomal escape, the results of our experiments reveal that the DOX in AG-Liposomes exhibited low fluorescence intensity in the central region and high fluorescence intensity in the peripheral region at 2 h. This implies that only a portion of the DOX had escaped the lysosomes. At 4 h, the DOX fluorescence distribution of in AG-Liposomes was relatively uniform, indicating that a significant portion of the DOX had completed lysosomal

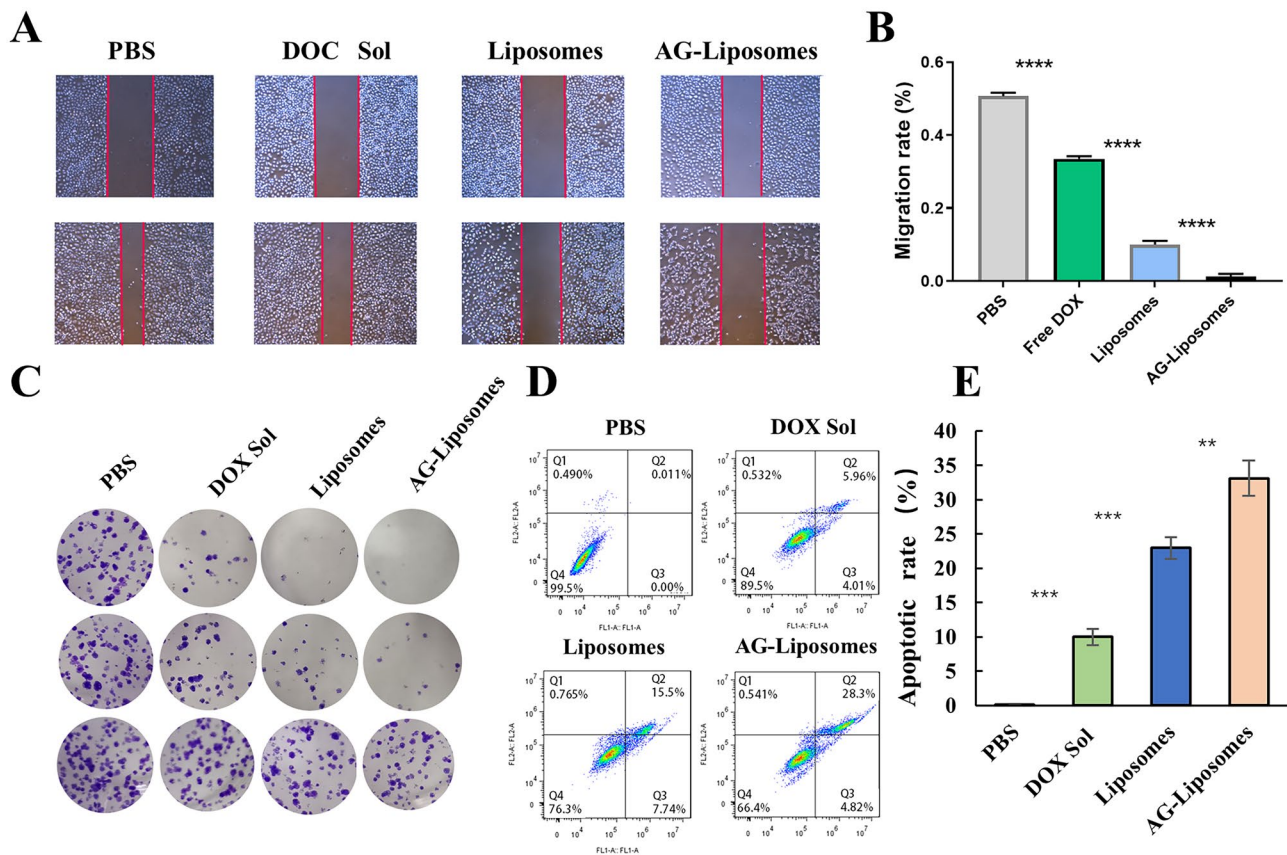


**Fig. 6** Images showing the detection of the cell migration, the cell clone formation and the cell apoptosis experiment: **A** Images of cell migration; **B** Statistical analysis of cell migration; **C** Images of the

cell clone formation; **D** Images of the cell apoptosis experiment and **E** Statistical analysis of the cell apoptosis rate (n=3). \*\*  $p < 0.01$ , \*\*\*  $p < 0.001$ , \*\*\*\*  $p < 0.0001$

escape and had entered the nucleus. However, at this time, some of the DOX fluorescence still overlapped with the fluorescence of the lysosomal dye, indicating that lysosomal escape was not completely achieved. In comparison, at 2 and 4 h, there was less overlap between the DOX and the nuclei in Liposomes, and most of the red fluorescence of the DOX was mainly scattered around the nuclei, which was in the same regions as the green fluorescence of the lysosomes. This result indicates that most of the DOX in the Liposomes had not yet completed lysosomal escape within 4 h.

### Western blot analysis

The expression of Bax, Bcl-2, cleaved caspase-9, and cleaved caspase-3 in MGC 803 cells was evaluated using GAPDH as the reference protein. All three DOX preparations changed these apoptosis-related proteins a lot (Fig. 8). Specifically, expressions of pro-apoptosis proteins (Bax, Cleaved caspase-9, and Cleaved caspase-3) were increased and the expression of anti-apoptosis protein (Bcl-2) was decreased, promoting tumor cell apoptosis. The order of effectiveness, from lowest to highest, was DOX solution,

Liposomes, and AG-Liposomes. As a result, AG-Liposomes are more efficient in inducing tumor cell apoptosis compared to the other two DOX preparations.

### Tumor inhibition experiment

Throughout the treatment period, we recorded the body weight of tumor-bearing mice, measured the tumor volume at regular intervals, weighed the tumor weight at the end of the experiment, and calculated the tumor inhibition rate. The body weight changes during the treatment (Fig. 9A) showed no significant difference among the groups. The HE staining analysis of heart, liver, spleen, lung, and kidney of each group (Fig. 9E) revealed no major organ damage caused by any formulation. Thus, the addition of AG-Chol did not increase the toxicity of DOX liposome.

The effect of the treatment on tumor volume is illustrated in Fig. 9B and the tumor tissue is presented in Fig. 9C. The final tumor volume and weight decreased gradually in DOX Sol, Liposomes and AG-Liposomes compared with the normal saline group. The tumor volume inhibition rates of DOX Sol, Liposomes and

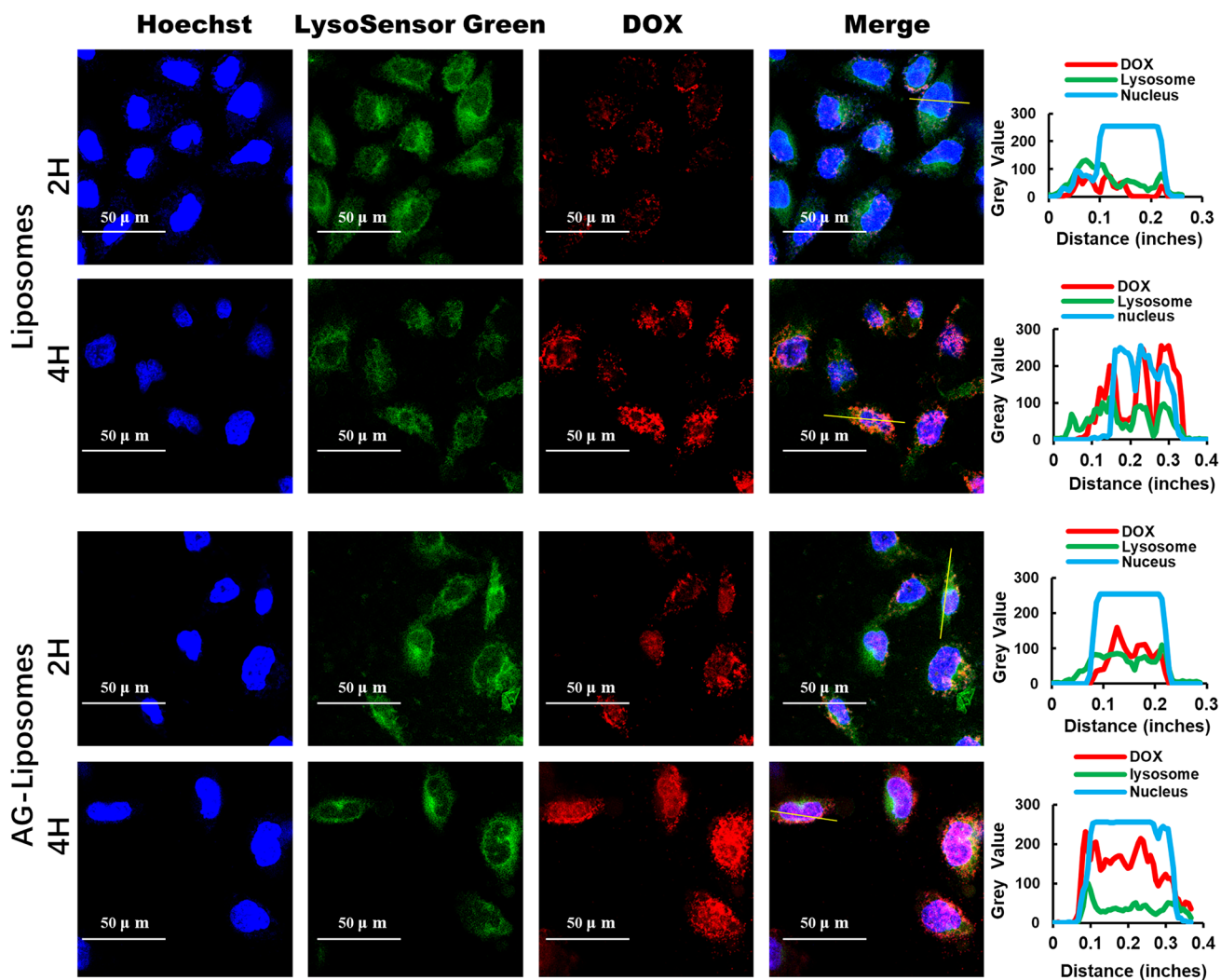


**Fig. 7** CLSM images of DOX-loaded liposomes in MGC 803 cells after 2 h and 4 h of incubation. For each panel, images from left to right show cell nuclei stained with Hoechst 33,342 (blue), lysosomes stained with LysoSensor Green (green), DOX (red), and their merge (bar = 50 μm)

AG-Liposomes were  $78.5 \pm 2.2\%$ ,  $88.58 \pm 1.9\%$  and  $95.6 \pm 1.5\%$  respectively, and the tumor weight inhibition rates were  $64.28 \pm 8.9\%$ ,  $81.70\% \pm 0.6\%$  and  $94.61 \pm 0.3\%$ , respectively (Fig. 9D). There was a consistent trend between the change of tumor weight and tumor volume for the three preparations.

It is concluded that intravenous nanomedicine has to overcome at least five obstacles to exert its effect on tumor cells, abbreviated as CAPIR (circulation, accumulation, penetration, internalization and drug release) [32, 33]. Only drugs that can cross these five steps can work on tumor cells. However, the very qualities that favor

**Fig. 8** WB result: **A** WB pictures of different groups of tumors; **B** Column graph and statistical analysis of WB data (n = 3). NS no significant difference, \*\*  $p < 0.01$ , \*\*\*  $p < 0.001$ , \*\*\*\*  $p < 0.0001$

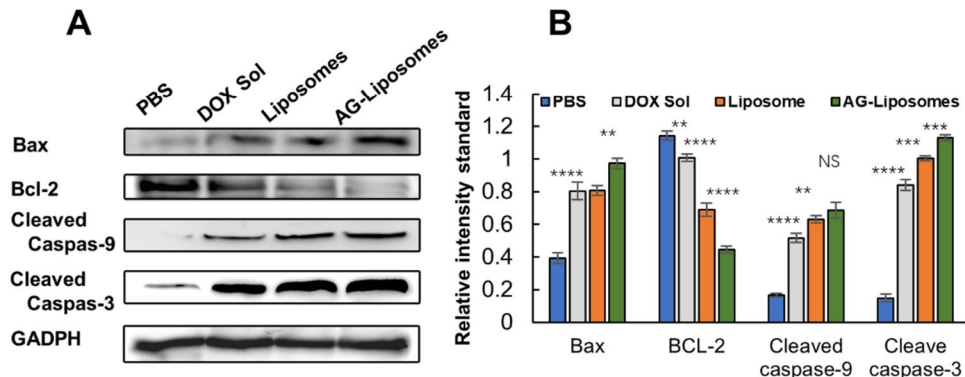
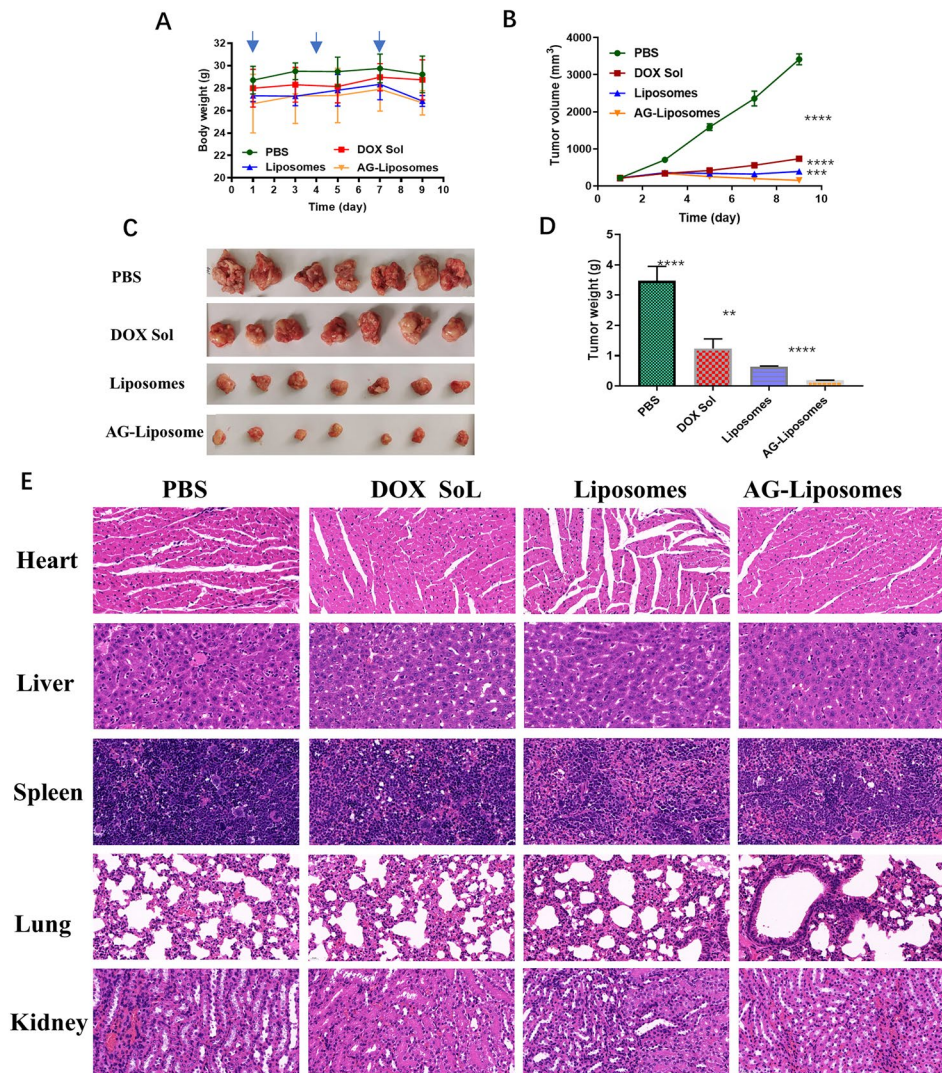




**Fig. 9** In vivo anti-tumor effect experiment: **A** Body weight of mice during treatment (n=7). Arrow indicates the time of treatment; **B** Tumor volume of mice during treatment (n=7); **C** Images of the dissected tumors; **D** Final tumor weight (n=7) and **E** HE staining of the main organs. \*\*  $p < 0.01$ , \*\*\*  $p < 0.001$ , \*\*\*\*  $p < 0.0001$



some of these steps are detrimental to others. For example, electrically neutral or negatively charged particles may be beneficial to the long cycle in phase C [33], but in the I and R phase, they are less effective than positively charged particles. The positive charge carried by the preparation we constructed has been verified in the previous animal experiments that after intravenous administration, more drugs enter the tumor tissue, so after the C and A stage, AG-Liposomes enter the tumor. In vitro release experiments demonstrated that AG-Liposomes were relatively stable at the pH of tumor tissue's intercellular substance. The uptake experiment and lysosomal escape experiment showed that if AG-Liposomes encounter tumor cells, they can be absorbed more rapidly and escape from lysosomes. It indicates that AG-Liposomes

also have great advantages in I and R phase. Therefore, compared with ordinary liposomes with negative charge, AG-Liposomes not only have advantages at the cellular level in vitro, but also can overcome many obstacles in animal experiments and achieve better anti-tumor effect than ordinary liposomes.

The results confirmed that AG-Chol modified liposomes could significantly enhance their anti-tumor effect in vivo compared with control liposomes at the animal level. Therefore, the advantages of the preparation in animal experiments and in vitro cytological experiments can also be further extrapolated to model animals. Overall, the addition of AG-Chol can enhance the targeting of liposomes to tumor tissues and the uptake of tumor cells, thus achieving a higher tumor inhibition rate.

## Conclusions and prospectives

We synthesized an agmatine-cholesterol conjugate (AG-Chol) that can replace cholesterol in preparing DOX liposomes. The compound could improve the tumor targeting of liposome preparations, promote the lysosomal escape of liposomes, decrease the distribution of liposomes in normal tissues, and showed a higher anti-tumor effect compared to the control. Thus, liposomal formulation prepared with AG-Chol has great potential for anti-tumor therapy.

Our practice also demonstrates that AG-Chol has a range of applications in nano-preparations [34]. It can not only be used to prepare liposomes, but also can be self-assembled into nanoparticles, or loaded into PLGA and other carriers. Interestingly, high concentrations of AG-Chol nanoparticles have gel properties, which may have some advantages in drug delivery. In addition, Agmatine itself is an endogenous polyamine that has a variety of effects [35, 36]. Therefore, AG-Chol has potential applications beyond being an excipient. The effects of AG-Chol on reducing blood glucose concentration, antidepressant activity, and reducing neuropathic pain effect remain to be investigated. However, the safety of AG-Chol and whether it has any other potential risks still needs to be fully elucidated through more experiments.

**Acknowledgements** We thank Pro. Xiaojing Shi for help with the automatic digital slide scanner.

**Authors' contributions** Yanzhi Wang, Jiabin Zheng and Hongmin Liu contributed to the study conception and design. Linchao wang performed the experiment, data collection and analysis. Hanyue Chang, Qing Shen, Sai zhang and Shanshan Sun helped to perform the experiment. Yanzhi wang wrote the manuscript and supervised the project. Yanzhi Wang, Ying Liu, Jiabin Zheng and Hongmin Liu gave financial or resource support for the project.

**Funding** This project received support from the National Natural Science Foundation of China (No.82020108030 and U21A20416), the Provincial Key Scientific Research Projects of Colleges and Universities of Henan (No. 21A350013), National Key Research Program of Proteins (No. 2018YFE0195100 for H.-M. L.), and General Project of Natural Science Foundation of Hainan Province (No. 821MS0826).

**Data availability** The authors confirm that the data supporting the findings of this study are available within the article.

## Declarations

**Ethics approval and consent to participate** All institutional and national guidelines for the care and use of laboratory animals were followed. This study was performed in line with the principles of the Declaration of Helsinki. Approval was granted by the Ethics Committee of Zhengzhou University (No: xyylsc20220065).

**Consent for publication** Not applicable.

**Competing interests** The authors declare no competing interests.

## References

- Kratz F. Albumin as a drug carrier: design of prodrugs, drug conjugates and nanoparticles. *J Control Release*. 2008;132(3):171–83.
- Jokerst JV, Lobovkina T, Zare RN, Gambhir SS. Nanoparticle PEGylation for imaging and therapy. *Nanomedicine (Lond)*. 2011;6(4):715–28.
- Kato T, Jin CS, Ujiie H, et al. Nanoparticle targeted folate receptor 1-enhanced photodynamic therapy for lung cancer. *Lung Cancer*. 2017;113:59–68.
- Zhang Y, Wang T, Tian Y, et al. Gold nanorods-mediated efficient synergistic immunotherapy for detection and inhibition of postoperative tumor recurrence. *Acta Pharm Sin B*. 2021;11(7):1978–92.
- Tran S, DeGiovanni PJ, Piel B, Rai P. Cancer nanomedicine: a review of recent success in drug delivery. *Clin Transl Med*. 2017;6(1):44.
- Wang C, Zhang Y, Dong Y. Lipid nanoparticle-mRNA formulations for therapeutic applications. *Acc Chem Res*. 2021;54(23):4283–93.
- He Y, Zhang W, Xiao Q, et al. Liposomes and liposome-like nanoparticles: From anti-fungal infection to the COVID-19 pandemic treatment. *Asian J Pharm Sci*. 2022;17(6):817–37.
- Suzuki Y, Ishihara H. Difference in the lipid nanoparticle technology employed in three approved siRNA (Patisiran) and mRNA (COVID-19 vaccine) drugs. *Drug Metab Pharmacokin*. 2021;41:100424.
- Labouta HI, Langer R, Cullis PR, et al. Role of drug delivery technologies in the success of COVID-19 vaccines: a perspective. *Drug Deliv Transl Res*. 2022;12(11):2581–8.
- Wang X, Li Y, Wang D, et al. Evaluation of antitumor efficacy of folate-poly(2-ethyl-2-oxazoline)-distearoyl phosphatidyl ethanolamine based liposome. *Pharm Dev Technol*. 2021;26(1):110–8.
- Du Y, He W, Xia Q, Zhou W, Yao C, Li X. Thioether Phosphatidylcholine Liposomes: A Novel ROS-Responsive Platform for Drug Delivery. *ACS Appl Mater Interfaces*. 2019;11(41):37411–20.
- Kibria G, Hatakeyama H, Sato Y, Harashima H. Anti-tumor effect via passive anti-angiogenesis of PEGylated liposomes encapsulating doxorubicin in drug resistant tumors. *Int J Pharm*. 2016;509(1–2):178–87.
- Gabizon A, Catane R, Uziely B, et al. Prolonged circulation time and enhanced accumulation in malignant exudates of doxorubicin encapsulated in polyethylene-glycol coated liposomes. *Cancer Res*. 1994;54(4):987–92.
- Tang J, Zhang L, Fu H, et al. A detachable coating of cholesterol-anchored PEG improves tumor targeting of cell-penetrating peptide-modified liposomes. *Acta Pharm Sin B*. 2014;4(1):67–73.
- Shi K, Zhao Y, Miao L, et al. Dual functional LipoMET mediates envelope-type nanoparticles to combinational oncogene silencing and tumor growth inhibition. *Mol Ther*. 2017;25(7):1567–79.
- Wang Y, Sun C, Huang L, et al. Magnolol-loaded cholesterol biguanide conjugate hydrochloride nanoparticles for triple-negative breast cancer therapy. *Int J Pharm*. 2022;615:121509.
- Pryor R, Norvaisas P, Marinos G, et al. Host-microbe-drug-nutrient screen identifies bacterial effectors of metformin therapy. *Cell*. 2019;178(6):1299–1312.e29.
- Nie Y, Ji L, Ding H, et al. Cholesterol derivatives based charged liposomes for doxorubicin delivery: preparation, in vitro and in vivo characterization. *Theranostics*. 2012;2(11):1092–103.
- Rodríguez-Pulido A, Martín-Molina A, Rodríguez-Beas C, Llorca O, Aicart E, Junquera E. A theoretical and experimental approach to the compaction process of DNA by dioctadecyldimethylammonium bromide/zwitterionic mixed liposomes. *J Phys Chem B*. 2009;113(47):15648–61.
- Rodríguez-Pulido A, Ortega F, Llorca O, Aicart E, Junquera E. A physicochemical characterization of the interaction between



- DC-Chol/DOPE cationic liposomes and DNA. *J Phys Chem B*. 2008;112(39):12555–65.
21. Vaupel P, Kallinowski F, Okunieff P. Blood flow, oxygen and nutrient supply, and metabolic microenvironment of human tumors: a review. *Cancer Res*. 1989;49(23):6449–65.
  22. Luo R, Li Y, He M, et al. Distinct biodistribution of doxorubicin and the altered dispositions mediated by different liposomal formulations. *Int J Pharm*. 2017;519(1–2):1–10.
  23. Chen HP, Tung FI, Chen MH, Liu TY. A magnetic vehicle realized tumor cell-targeted radiotherapy using low-dose radiation. *J Control Release*. 2016;226:182–92.
  24. Wang M, Li J, Li X, et al. Magnetically and pH dual responsive dendrosomes for tumor accumulation enhanced folate-targeted hybrid drug delivery. *J Control Release*. 2016;232:161–74.
  25. Yu Z, Ge Y, Sun Q, et al. A pre-protective strategy for precise tumor targeting and efficient photodynamic therapy with a switchable DNA/upconversion nanocomposite. *Chem Sci*. 2018;9(14):3563–9.
  26. Wang M, Guo Y, Xue Y, et al. Engineering multifunctional bioactive citric acid-based nanovectors for intrinsic targeted tumor imaging and specific siRNA gene delivery in vitro/in vivo. *Biomaterials*. 2019;199:10–21.
  27. Song W, Shen L, Wang Y, et al. Synergistic and low adverse effect cancer immunotherapy by immunogenic chemotherapy and locally expressed PD-L1 trap. *Nat Commun*. 2018;9(1):2237.
  28. Qu D, Jiao M, Lin H, et al. Anisamide-functionalized pH-responsive amphiphilic chitosan-based paclitaxel micelles for sigma-1 receptor targeted prostate cancer treatment. *Carbohydr Polym*. 2020;229:115498.
  29. Wu J, Hu X, Liu R, Zhang J, Song A, Luan Y. pH-responsive and self-targeting assembly from hyaluronic acid-based conjugate toward all-in-one chemo-photodynamic therapy. *J Colloid Interface Sci*. 2019;547:30–9.
  30. Yoon HY, Koo H, Choi KY, et al. Tumor-targeting hyaluronic acid nanoparticles for photodynamic imaging and therapy. *Biomaterials*. 2012;33(15):3980–9.
  31. Chen S, Zhou Q, Wang G, et al. Effect of cationic charge density on transcytosis of polyethylenimine. *Biomacromol*. 2021;22(12):5139–50.
  32. Sun Q, Zhou Z, Qiu N, Shen Y. Rational design of cancer nanomedicine: nanoproperty integration and synchronization. *Adv Mater*. 2017;29(14).
  33. Alexis F, Pridgen E, Molnar LK, Farokhzad OC. Factors affecting the clearance and biodistribution of polymeric nanoparticles. *Mol Pharm*. 2008;5(4):505–15.
  34. Wang Y, Zheng J, Wang L, et al. A cholesterol monoguanidine conjugate and its preparation method and application: CN. Patent 202110801820.0. 2021-07-15.
  35. Piletz JE, Aricioglu F, Cheng JT, et al. Agmatine: clinical applications after 100 years in translation. *Drug Discov Today*. 2013;18(17–18):880–93.
  36. Watts D, Pfaffenseller B, Wollenhaupt-Aguiar B, Paul Géa L, Cardoso TA, Kapczinski F. Agmatine as a potential therapeutic intervention in bipolar depression: the preclinical landscape. *Expert Opin Ther Targets*. 2019;23(4):327–39.

**Publisher's Note** Springer Nature remains neutral with regard to jurisdictional claims in published maps and institutional affiliations.

Springer Nature or its licensor (e.g. a society or other partner) holds exclusive rights to this article under a publishing agreement with the author(s) or other rightsholder(s); author self-archiving of the accepted manuscript version of this article is solely governed by the terms of such publishing agreement and applicable law.